
Semantic One-Dimensional Tokenizer for Image Reconstruction and Generation

Yunpeng Qu^{*1} Kaidong Zhang^{*2} Yukang Ding² Ying Chen² Jian Wang¹

Abstract

Visual generative models based on latent space have achieved great success, underscoring the significance of visual tokenization. Mapping images to latents boosts efficiency and enables multimodal alignment for scaling up in downstream tasks. Existing visual tokenizers primarily map images into fixed 2D spatial grids and focus on pixel-level restoration, which hinders the capture of representations with compact global semantics. To address these issues, we propose **SemTok**, a semantic one-dimensional tokenizer that compresses 2D images into 1D discrete tokens with high-level semantics. SemTok sets a new state-of-the-art in image reconstruction, achieving superior fidelity with a remarkably compact token representation. This is achieved via a synergistic framework with three key innovations: a 2D-to-1D tokenization scheme, a semantic alignment constraint, and a two-stage generative training strategy. Building on SemTok, we construct a masked autoregressive generation framework, which yields notable improvements in downstream image generation tasks. Experiments confirm the effectiveness of our semantic 1D tokenization. Our code will be open-sourced.

1. Introduction

Visual generative models based on diffusion models (Romach et al., 2022; Ho et al., 2020; Chen et al., 2023; Dhariwal & Nichol, 2021a) or autoregressive modeling (AR) (Chang et al., 2022; Tian et al., 2024; Sun et al., 2024; Xie et al., 2024) have achieved significant success and are widely used in creative applications. These models typically operate in a latent space rather than pixel space, using a tokenizer to map images to continuous (Kingma & Welling, 2013) or discretized (Esser et al., 2021) representations. Latent

representations are more compact and expressive than raw pixels, simplifying complexity and facilitating integration with multimodal data (Yu et al., 2024).

While image tokenizers like VQGAN (Esser et al., 2021) achieve great success in visual generation and understanding tasks, they adhere to the standard spatial structure assumption, representing images as two-dimensional (2D) spatial grids (Wang et al., 2025). The rigid spatial positioning of grid-based tokens biases them towards capturing local semantics, which hinders the formation of a compact, globally-aware image representation due to inherent local redundancies. Such 2D representations also limit their applicability to downstream tasks, as tokens are typically flattened into one-dimensional (1D) form in generation frameworks, making it more complex to model spatial structures. Moreover, the bidirectional spatial correlations of 2D tokens cannot model causal dependencies as in language (Tian et al., 2024).

Besides, existing visual tokenizers are trained on image reconstruction tasks, with losses aimed at optimizing pixel-level reconstruction errors (Van Den Oord et al., 2017). This causes the model to prioritize low-level texture reconstruction over high-level semantic representation, which limits both information density and the low-entropy optimization of the distribution. While the integration of LPIPS (Zhang et al., 2018) and GAN (Goodfellow et al., 2020) losses enhances fidelity, such losses backpropagate indirectly from the decoder to the encoder, lacking the direct constraint on the encoder’s inherent representation capability, which is crucial for integration with LLM-based understanding and generative frameworks (Wang et al., 2024; Ge et al., 2024).

The aforementioned limitations underscore the need for a more advanced tokenizer, raising a key research question: *how can we design a tokenizer that yields more compact and semantically richer representations?* We believe that compact representations stem from the low-entropy optimization of the latent space, as compressed tokens should exhibit more clustered distributions to capture more discriminative and representative semantics. This motivates us to develop a more compact tokenization scheme from three aspects: (1) **Tokenization form**: Inspired by prior works (Yu et al., 2024; Bachmann et al., 2025; Wang et al., 2025) that compress images into 1D sequences, we highlight the value of 1D visual representations, which enable tokens to priori-

^{*}Equal contribution ¹Tsinghua University, Beijing, China
²Alibaba Group, Beijing, China. Correspondence to: Yukang Ding <dingyukang.dyk@taobao.com>, Jian Wang <jianwang@tsinghua.edu.cn>.

tize critical global semantics while eliminating redundancy among local information. (2) **Tokenization constraint**: It is necessary to impose explicit distributional constraints on the encoder side, so as to drive compressed tokens toward more distinct and concentrated semantic representations. (3) **Tokenization training paradigm**: We aim at exploring a more diverse latent space via a generative training paradigm to avoid potential distribution collapse of the latent space from pixel-level reconstruction.

In this paper, we introduce a **Semantic one-dimensional Tokenizer (SemTok)**, which compresses the image into a 1D discrete sequence imbued with high-level semantics, and reconstructs the image via a generative decoder. To realize the 1D tokenization form, we leverage the *2D-to-1D conversion framework* based on MMDiT (Esser et al., 2024) to encode the semantics of 2D images into compact 1D tokens. To concentrate the latent distribution, we introduce a *semantic alignment constraint* to directly supervise the encoder in generating clustered tokens aligned with multimodal inputs, boosting downstream representational capacity. To explore a more diverse latent space, we propose a *two-stage generative training strategy* involving generative pre-training and refinement-oriented fine-tuning, to acquire generative priors and improve reconstruction.

Furthermore, the compression paradigm of the tokenizer dictates the form of AR-based image generation, such as the next-token (Ramesh et al., 2021; Yu et al., 2022b) prediction or next-scale prediction (Tian et al., 2024) with 2D tokenizers. Building upon SemTok, we explore an AR paradigm tailored for 1D sequences. Leveraging their inherent global semantics and close interconnectivity, we construct a masked autoregressive approach to enable high-quality visual generation. SemTok and the AR model yield distinct improvements in image reconstruction and downstream image generation tasks, demonstrating the potential of semantic 1D tokenization. Our contributions are as follows:

1. We propose SemTok, a novel visual tokenizer that compresses 2D images into 1D token sequences with compact high-level semantic representations. Our SemTok achieves state-of-the-art (SOTA) performance on image reconstruction tasks.
2. Our SemTok improves three key areas: tokenization form, tokenization constraints, and training framework. It validates 1D tokenization and semantic alignment for compact representations, while a generative pipeline enhances the semantic diversity of the latent space.
3. Building upon SemTok, we construct a masked autoregressive modeling framework for generation with highly competitive performance, which demonstrates the advantages of global 1D semantic tokenization in downstream image generation tasks.

2. Related work

Image Tokenization. Visual tokenizers project images or videos into compact latent spaces while preserving key visual information. VAE (Kingma & Welling, 2013) maps images to continuous distributions, while VQVAE (Van Den Oord et al., 2017; Razavi et al., 2019) further refines this by quantizing to form discrete vectors. Subsequent works make improvements in training objectives (Ramesh et al., 2021; Esser et al., 2021; Yu et al., 2021), multiple quantization (Lee et al., 2022; Zheng et al., 2022), and quantization techniques (Mentzer et al., 2023; Zhao et al., 2024; Yu et al., 2023), aiming to enhance reconstruction quality and facilitate downstream tasks. However, these works compress images into 2D maps with fixed spatial positions, limiting the scope of semantic representation.

Titok (Yu et al., 2024) abandons 2D structure preservation by representing images with learnable 1D tokens, a paradigm extended in works like FlowMo (Sargent et al., 2025), FlexTok (Bachmann et al., 2025), and SelfTok (Wang et al., 2025). These works offer new insights into visual tokenizers, yet they may still rely on priors from 2D tokenizers or impose sequential dependencies on tokens. More critically, these works remain optimized for end-to-end image reconstruction, emphasizing low-level features over high-level semantics, which hinders compact visual representations and their integration with vision-language models (VLMs) (Li et al., 2023a; Liu et al., 2023a; Sun et al., 2023; Jin et al., 2024). VA-VAE (Yao et al., 2025) and many related works (Ma et al., 2025; Zhao et al., 2025) have shown that a pretrained semantic encoder like CLIP (Radford et al., 2021) can achieve concentrated semantic representations and demonstrate strong potential for high-quality generation (Zheng et al., 2025). In this work, we revisit how to achieve more compact semantic representations and propose an advanced tokenizer by jointly improving the tokenization form, the tokenization constraints, and the training paradigm.

Autoregressive Modeling for Generation. Diffusion-based image generation (Dhariwal & Nichol, 2021b; Hoogeboom et al., 2023; Peebles & Xie, 2023; Yang et al., 2025) has achieved remarkable success, while visual autoregressive modeling (Tian et al., 2024; Li et al., 2024; Han et al., 2025; Yu et al., 2025) has recently gained traction, delivering comparable results in many generation tasks. These autoregressive methods rely on pre-defined visual tokenizers (e.g., VQVAE (Yu et al., 2022a)) to generate images in a step-by-step fashion in 2D sequences. We argue that autoregressive generation on 1D tokens is superior compared to 2D tokens, as it captures more compact global semantics for stronger coherence, whereas 2D tokens are constrained by isolated local semantics. Inspired by bidirectional transformers (Weber et al., 2024; Zheng et al., 2022; Devlin et al., 2019), we further advocate for masked autoregression, as

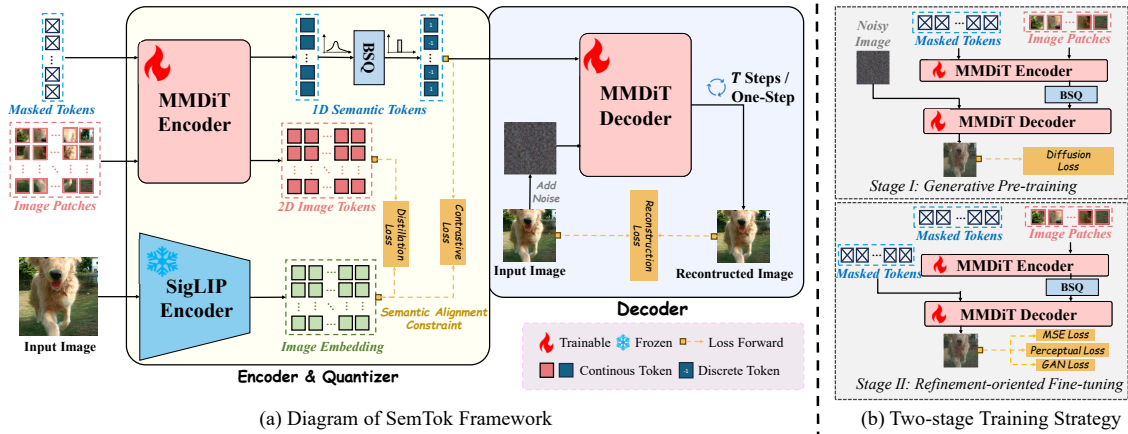


Figure 1. An overview of SemTok. (a) SemTok compresses 2D images into 1D discrete tokens through the encoder and reconstructs images through the decoder. A *semantic alignment constraint* is introduced at the encoder end for compact semantic representations. (b) To explore the semantic diversity of the latent space, SemTok adopts a two-stage training strategy: in Stage I, a diffusion-based decoder is used to predict images from noise; in Stage II, a one-step refiner is trained on image reconstruction tasks to enhance texture details.

1D sequences do not inherently possess nor require the imposition of causal dependencies. In this paper, building on our SemTok, we explore autoregressive modeling over 1D semantic representations for image generation.

3. Methods

We propose SemTok, a novel semantic one-dimensional tokenizer for compact visual representations. To this end, our SemTok is guided by five core principles that enable effective compression of key visual semantics while ensuring strong scalability across a wide range of downstream tasks.

- 1D sequence for global semantics.** SemTok compresses images into 1D representations to avoid redundancy from 2D positional constraints, enabling tokens to capture global semantics and form a compact latent space with strong inter-token correlations.
- Semantic representations for clustered distribution.** Tokenizers trained on reconstruction yield low-capacity latents rich in local details but poor in global semantics. Explicit constraints are essential to encourage clustered distributions that encode discriminative information.
- Non-sequential modeling for bidirectional correlations.** Compressed tokens encode complementary semantics with bidirectional dependencies rather than Markovian ones, requiring non-sequential modeling to preserve global correlations without causal constraints.
- Discrete vectors for semantic disentanglement.** Discrete vectors offer clearer semantic disentanglement than continuous latents (Wang et al., 2025), enabling easy convergence in the discrete space and allowing us to adopt the LLMs’ successful training paradigm.

5. Generative training for latent space exploration.

Pixel-level reconstruction may cause distribution collapse and oversmoothed outputs. Generative training enables the tokenizer to explore a more diverse latent space, allowing sequences to capture richer semantics.

Based on the principles, in Fig.1, we construct the Semtok framework, which consists of three main components. (1) An encoder \mathcal{E} compresses the image $I \in \mathbb{R}^{H \times W \times 3}$ into 1D tokens $z \in \mathbb{R}^{K \times d}$. (2) A quantizer \mathcal{Q} looks up the continuous latents z into discrete vectors \bar{z} . (3) A decoder \mathcal{D} generates the reconstructed image \hat{I} given \bar{z} .

3.1. 1D Tokenization with Semantic Alignment

Encoder with Semantic Alignment Constraint. Our encoder utilizes an MMDiT-based backbone (Esser et al., 2024) to achieve the 2D-to-1D conversion, which excels at processing and integrating multimodal inputs (e.g., 2D images and 1D text sequences) through different branches. We regard 1D tokens as a distinct semantic modality, making 2D-to-1D conversion a natural multimodal alignment task that aligns well with MMDiT’s design. This dual-stream architecture naturally decomposes 1D tokenization: the 2D branch extracts semantic information, co-attention mechanisms compress it into the 1D branch, and the 1D branch re-integrates the semantics into a structured representation. We first use the pre-trained VAE of SD3.5 (Esser et al., 2024) to transform the images I into latents $x_v \in \mathbb{R}^{\frac{H}{f} \times \frac{W}{f} \times D}$ with downscale factor $f = 8$, where x_v is then be pacified as the input of one branch. The other branch inputs a series of learnable embeddings $z_m \in \mathbb{R}^{K \times d}$ as masked tokens.

As discussed earlier, we impose explicit constraints in the encoder to align high-level semantics and ensure a more

compact distribution of visual representations. Specifically, we introduce a semantic encoder SigLIP (Tschannen et al., 2025; Zhai et al., 2023) \mathcal{E}_{sig} , which has undergone extensive pre-training for language-image alignment, proven effective in understanding tasks, and thus boasts strong cross-modal alignment and semantic extraction capabilities. The outputs of our MMDiT encoder and SigLIP encoder are defined as:

$$x, z = \mathcal{E}(x_v, z_m), \quad x_{sig} = \mathcal{E}_{sig}(I), \quad (1)$$

where $x_{sig} \in \mathbb{R}^{\frac{H}{F} \times \frac{W}{F} \times C}$ is spatially aligned with x . Our *semantic alignment constraint* is divided into two parts, acting on both encoder branches. In the 2D image branch, we introduce spatial-aligned distillation loss for high-level semantic extraction. In the 1D token branch, we pool x_{sig} and use contrastive learning loss to associate pairs for the same sample and separate pairs that are not, ensuring the semantics are effectively conversed. We use quantized results $\mathcal{Q}(z)$ of z herein to compensate for quantization losses.

$$\begin{aligned} \mathcal{L}_{distill} &= \|x_{sig} - \mathbf{w}_x(x)\|^2, \\ \bar{z} = \mathcal{Q}(z), \mathbf{u} &= \frac{\mathcal{P}(x_{sig})}{\|\mathcal{P}(x_{sig})\|_2}, \quad \mathbf{v} = \frac{\mathbf{w}_z(\bar{z})}{\|\mathbf{w}_z(\bar{z})\|_2}, \\ \mathcal{L}_{contra}(\mathbf{v}, \mathbf{u}) &= \sum_{\mathbf{v} \in \mathcal{V}} \left(\log \frac{e^{t\mathbf{v}^\top \mathbf{u}}}{\sum_{\mathbf{u} \in \mathcal{U}} e^{t\mathbf{v}^\top \mathbf{u}}} \right), \\ \mathcal{L}_{sem} &= \mathcal{L}_{contra} + \mathcal{L}_{distill}, \end{aligned} \quad (2)$$

where \mathcal{P} is the pooling function, \mathcal{U}, \mathcal{V} are collections of samples in a batch, and $\mathbf{w}_x(\cdot), \mathbf{w}_z(\cdot)$ are projection weights. *Semantic alignment constraint* yields strong visual representations, better suited for advanced visual generation tasks.

Binary Spherical Quantizer. The quantizer maps continuous latents z to the closest discrete vector \bar{z} in the codebook \mathcal{C} , using a straight-through estimator (STE) (Bengio et al., 2013) to backpropagate through the quantization bottleneck. Increasing the codebook size reduces quantization error but significantly increases memory usage. Therefore, we employ the Binary Spherical Quantizer (BSQ) (Zhao et al., 2024), akin to Look-up-Free Quantization (LFQ) (Yu et al., 2023), where each channel dimension is mapped to every corner of a hypersphere through binary transformation, with the vector \bar{z} itself also serving as the codebook index k .

$$\mathcal{Q}(z) = \frac{1}{\sqrt{d}} \text{sign}\left(\frac{z}{\|z\|}\right), \quad k = \sum_{i=0}^d \mathbb{1}(\bar{z}_i > 0) \cdot 2^{i-1}, \quad (3)$$

Therefore, the codebook size of BSQ grows exponentially with channel dimension, with $|\mathcal{C}| = 2^d$. Unlike traditional VQ quantization, BSQ does not require storing a codebook, making it more suitable for scaling up. To optimize for effective quantization and encourage codebook utilization, an entropy objective is used as the loss (Jansen et al., 2020):

$$\mathcal{L}_{quant} = \mathbb{E}[H(\mathcal{Q}(z))] - H(\mathbb{E}[\mathcal{Q}(z)]). \quad (4)$$

where $H(\cdot)$ represents the entropy function.

Decoder. Our decoder also utilizes an MMDiT-based architecture. Since image reconstruction is a generative task for the decoder and requires strong generative priors to capture a richer semantic spectrum (Wang et al., 2025), we employ a decoder with larger parameters than the encoder and initialize its parameters from SD3.5 (Esser et al., 2024). We apply Relative Positional Encoding (RoPE) (Su et al., 2024) to better represent positional relationships.

3.2. Two-stage Training for Image Reconstruction

To explore a richer semantic distribution in the latent space, we design a two-stage generative training strategy, where the decoder generates images from noise or masked tokens.

Generative Pre-training. Pixel-level reconstruction constraints, aimed at optimizing fidelity, tend to converge to an overly smoothed latent space, making it difficult to generate semantically rich and realistic textures (Karras et al., 2019). To better explore the latent space, we first employ diffusion-based generative pre-training, as it optimizes the likelihood $p(\hat{I}|z)$ across all noise scales, preserving multiple distribution paths instead of collapsing to a single solution (Rombach et al., 2022). Diffusion-based decoders, leveraging the principled probabilistic modeling of the Evidence Lower Bound (ELBO), can more effectively capture the richness and diversity of semantic patterns (Chen et al., 2025). Building on flow matching (Liu et al., 2023b), the decoder models the velocity distribution from noisy image latents x_t , with noise ϵ and time $t \in [0, 1]$. The objective is as follows:

$$\begin{aligned} x_t &= t\epsilon + (1-t)x_v, \\ \mathcal{L}_{diff} &= \mathbb{E} \left[\|x_v - \epsilon - \mathcal{D}(x_t, \bar{z}, t)\|^2 \right], \end{aligned} \quad (5)$$

In the generative training, we jointly optimize the encoder \mathcal{E} , quantizer \mathcal{Q} , and decoder \mathcal{D} with the objective as:

$$\min \mathcal{L}_{diff} + \lambda_q \mathcal{L}_{quant} + \lambda_s \mathcal{L}_{sem}, \quad (6)$$

Flow-matching pre-training yields a more diverse latent space as a prior for image reconstruction, enabling encoded tokens z to maximally represent high-level semantics.

Refinement-oriented Fine-tuning. Although the first-stage pretraining yields a rich latent space, its fidelity objective is optimized in the latent space rather than the image space, ignoring the compression loss incurred during the pixel-to-latent encoding. Such manipulation degrades the generation of fine textures, where the inherent limitations of VQVAE restrict the tokenizer’s capacity ceiling. Moreover, the diffusion-based decoder incurs a high inference cost due to iterative sampling. Therefore, we conduct refinement-oriented training to achieve superior image reconstruction.

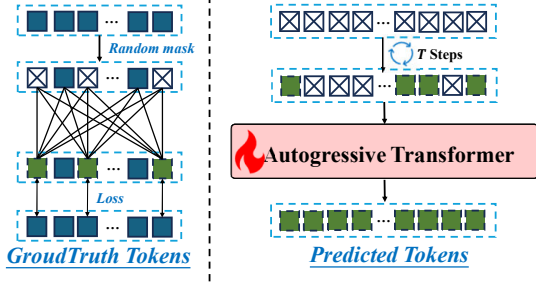


Figure 2. Illustration of masked autoregressive modeling of image generation with SemTok. (left) During training, we randomly mask several tokens and utilize bidirectional attention to allow each token to see all tokens, thereby perceiving global semantics. (right) During inference, the model predicts multiple tokens simultaneously in a random order until the complete sequence is filled.

In the decoder, the input of the original 2D noise branch is replaced by a sequence of learnable masked tokens z_m , directly reconstructing the image latent. The original diffusion v -prediction loss in the optimization objective is replaced with pixel-level reconstruction loss, which includes the MSE, perceptual, and GAN losses (Goodfellow et al., 2020), enabling SemTok to address potential detail losses resulting from latent compression adaptively.

$$\begin{aligned} \hat{I} &= \mathcal{D}(\bar{z}, z_m), \\ \min \mathcal{L}_{rec} &= \|I - \hat{I}\|^2 + \lambda_p \mathcal{L}_{per}(I, \hat{I}) + \lambda_G \mathcal{L}_G(I, \hat{I}). \end{aligned} \quad (7)$$

Following (Lipman et al., 2022) and (Weber et al., 2024), besides the classical LPIPS (Zhang et al., 2018), we incorporate ResNet (He et al., 2016) loss into the perceptual loss to further enhance reconstruction performance.

3.3. Autoregression for Image Generation

A proficient tokenizer benefits downstream generative tasks via exceptional image representation. Leveraging SemTok, we build an AR framework to validate our semantic 1D tokenization for image generation. SemTok compresses images into a compact token sequence that serves as constituents of global semantics, exhibiting stronger mutual dependencies. This enables greater gains in autoregressive generation, as previously generated tokens provide a stronger prior for subsequent ones. Since our 1D tokenization models bidirectional dependencies between tokens rather than sequential Markovian ones, it enables parallel token prediction with global context, thereby expanding the inherently unidirectional receptive scope of next-token prediction. Following MaskGIT (Chang et al., 2022), MAR (Li et al., 2024), and Muse (Chang et al., 2023), we adopt bidirectional transformers for masked autoregressive modeling.

As shown in Fig. 2, during training, we mask tokens in \bar{z} randomly with a binary mask M to form a masked token

sequence z_m . The transformer θ with bidirectional attention enables mutual perception between masked and known tokens, predicting the distribution probabilities of masked tokens. During inference, at the n -th step across N iterative steps, the transformer θ predicts the masked tokens \hat{z}^n at several random positions based on the current known tokens $(\hat{z}^1, \dots, \hat{z}^{n-1})$ and binary mask M_n . The framework updates the token sequence and binary mask, gradually transitioning from a sequence of masked tokens to semantic tokens, accelerating inference by generating multiple tokens simultaneously. The process is defined as follows:

$$\begin{aligned} \hat{z}^n &= (M_{n-1} \oplus M_n) \circ \theta(\hat{z}^1, \dots, \hat{z}^{n-1}), \\ p(\hat{z}^1, \dots, \hat{z}^N) &= \prod_n^N p(\hat{z}^n | \hat{z}^1, \dots, \hat{z}^{n-1}). \end{aligned} \quad (8)$$

4. Experimental Results

4.1. Implementation Details

Image Reconstruction We train and evaluate tokenizers on ImageNet-1k (Deng et al., 2009) at 256x256 resolution using standard metrics: rFID (Heusel et al., 2017), PSNR, SSIM, and LPIPS (Zhang et al., 2018). We provide the codebook size $|C|$, token length K , and Bits-per-pixel as the compression ratio $\frac{\log_2(|C|) \cdot K}{HW}$. SemTok employs FSQ (Zhao et al., 2024) for quantization, differing from VQ (Van Den Oord et al., 2017) by not needing extra codebook storage. We provide two models with different codebook sizes to evaluate their impact on the reconstruction quality.

Images are compressed using SD3.5-VAE (Rombach et al., 2022) with a downscale factor of 8 into quantized tokens with length 256. The hyperparameters $\lambda_q, \lambda_s, \lambda_p, \lambda_G$ are set to 0.0025, 0.05, 0.1, 0.1, respectively. We train SemTok for 200k iterations in Stage I with batchsize 256 and 100k iterations in Stage II with batchsize 64, using AdamW with learning rate of 5×10^{-5} and weight decay of 1×10^{-3} .

Image Generation. We build a masked autoregressive framework based on SemTok and evaluate it on class-conditional image generation using ImageNet-1k (256x256) (Deng et al., 2009). We report standard metrics: gFID (Heusel et al., 2017), Inception Score (IS) (Salimans et al., 2016), Precision, and Recall (Kynkäänniemi et al., 2019).

AR model adopts the LLamaGen (Sun et al., 2024) with bidirectional attention. It is trained for 800k iterations with batchsize 2048, using AdamW with learning rate of 2×10^{-4} and weight decay of 0.03. During training, we randomly sample a ratio from [0.7, 1.0] to mask semantic tokens (He et al., 2022; Li et al., 2024). At inference, tokens are filled in random masked positions over 64 steps via cosine annealing, with Classifier-Free Guidance (CFG) (Ho & Salimans, 2022) applied at a linearly increased scale of 6.0.

Table 1. Reconstruction results of SOTA tokenizers on ImageNet (256 × 256). *: indicates a continuous tokenizer trained on OpenImages. -re: indicates the use of rejection sampling.

Tokenizer	Type	Quant	#Bits-per-pixel	#Token	#Codebook	rFID↓	PSNR↑	SSIM↑	LPIPS↓
Taming VQ-GAN-re (Esser et al., 2021)	2D	VQ	0.055	16×16	2 ¹⁴	4.98	-	-	-
LlamaGen-16 (Sun et al., 2024)	2D	VQ	0.055	16×16	2 ¹⁴	2.19	20.67	0.589	0.132
MaskBiT (Weber et al., 2024)	2D	LFQ	0.055	16×16	2 ¹⁴	1.37	21.50	0.560	-
Cosmos DI-16x16 (Agarwal et al., 2025)	2D	FSQ	0.062	16×16	≈ 2 ¹⁶	4.40	19.98	0.536	0.153
OpenMagViT-V2 (Luo et al., 2024)	2D	LFQ	0.070	16×16	2 ¹⁸	1.17	21.63	0.640	0.111
VAR (Tian et al., 2024)	2D	VQ	0.125	680	2 ¹²	0.99	22.12	0.624	0.109
RQ-VAE (Lee et al., 2022)	2D	VQ	0.055	8×8×4	2 ¹⁴	3.20	-	-	-
ViT-VQGAN (Yu et al., 2021)	2D	VQ	0.203	32×32	2 ¹³	1.28	-	-	-
SD-VAE* (Rombach et al., 2022)	2D	KL	1.000	32*32	-	1.35	21.99	0.628	0.098
TiTok-L-32 (Yu et al., 2024)	1D	VQ	0.006	32	2 ¹²	2.21	15.60	0.359	0.322
TiTok-B-64 (Yu et al., 2024)	1D	VQ	0.012	64	2 ¹²	1.70	16.80	0.407	0.252
TiTok-S-128 (Yu et al., 2024)	1D	VQ	0.023	128	2 ¹²	1.71	17.52	0.437	0.210
FlexTok (Bachmann et al., 2025)	1D	FSQ	0.062	256	64,000	1.45	18.53	0.465	0.222
FlowMo-Lo (Sargent et al., 2025)	1D	LFQ	0.070	256	2 ¹⁸	0.95	22.07	0.649	0.113
SemTok (Ours)	1D	BSQ	0.070	256	2 ¹⁸	0.88	22.19	0.639	0.128
SemTok (Ours)	1D	BSQ	0.125	256	2 ³²	0.67	23.05	0.684	0.100



Figure 3. Comparison of reconstructions from different tokenizers.

4.2. Image Reconstruction

Quantitative results. Quantitative results for image reconstruction are shown in Tab. 1. Compared to conventional 2D and 1D tokenizers, SemTok achieves superior rFID and PSNR at the same Bits-per-pixel of 0.070. This gain stems from SemTok’s unique design: by enforcing *semantic alignment constraint* and representing images as compact 1D high-level tokens, it captures global structure more effectively while avoiding the redundancy and local bias of pixel-aligned 2D grids. By further increasing the codebook size to expand representational capacity without adding storage, SemTok achieves consistent improvements and **attains SOTA results across most metrics with an impressive 0.67 rFID on ImageNet**, even surpassing the continuous VAE tokenizer of SD-v2.1 (Rombach et al., 2022).

Qualitative results. In Fig. 3, we visualize some reconstruction results between different tokenizers from the test set. Our SemTok consistently generates images with accurate semantics and fine-grained texture details, aligning with the metrics in Tab. 1. For example, SemTok demonstrates superior structural fidelity over other tokenizers, excelling in creating intricate animal fur, facial features, and detailed structures. The results highlight SemTok’s strong capability to compress accurate semantic representations and generate realistic images, even under a compact compression ratio.

4.3. Image Generation

Based on SemTok, we build a masked autoregressive framework for image generation and compare it against previous GAN-based, diffusion-based, or AR-based methods, with

Fully Generated images *with VQGAN tokenizer*



Fully Generated images *with SemTok tokenizer*



Figure 4. Generation results with different tokenizers.

Table 2. Generation results with other methods on ImageNet (256 × 256). *: indicates generating images at resolution 384 × 384 and resizing back to 256 × 256.

Generator	Type	Params	gFID↓	IS ↑	Pre↑	Rec↑
BigGAN (Brock et al., 2018)	GAN	112M	6.95	224.5	0.89	0.38
GigaGAN (Kang et al., 2023)	GAN	569M	3.45	225.5	0.84	0.61
LDM-4-G (Rombach et al., 2022)	Diff.	400M	3.60	247.7	-	-
DiT-L/2 (Peebles & Xie, 2023)	Diff.	458M	5.02	167.2	0.75	0.57
DiT-XL/2 (Peebles & Xie, 2023)	Diff.	675M	2.27	278.2	0.83	0.57
VDM++ (Kingma & Gao, 2023)	Diff.	2.0B	2.12	267.7	-	-
VQGAN (Esser et al., 2021)	AR	1.4B	15.78	78.3	-	-
RQ-Tran. (Lee et al., 2022)	AR	3.8B	3.80	323.7	-	-
ViTVQ (Yu et al., 2021)	AR	1.7B	4.17	175.1	-	-
LlamaGen-L* (Sun et al., 2024)	AR	343M	3.07	256.1	0.83	0.52
LlamaGen-XL* (Sun et al., 2024)	AR	775M	2.62	244.1	0.80	0.57
LlamaGen-XXL* (Sun et al., 2024)	AR	1.4B	2.34	253.9	0.80	0.59
LlamaGen-3B* (Sun et al., 2024)	AR	3.1B	2.18	263.3	0.81	0.58
RandAR-L (Pang et al., 2025)	AR	343M	2.55	288.8	0.81	0.58
RandAR-XL (Pang et al., 2025)	AR	775M	2.25	317.8	0.80	0.60
RandAR-XXL (Pang et al., 2025)	AR	1.4B	2.15	322.0	0.79	0.62
Open-MAGVIT2-B (Luo et al., 2024)	AR	343M	3.08	258.3	0.85	0.51
Open-MAGVIT2-L (Luo et al., 2024)	AR	804M	2.51	271.7	0.84	0.54
Open-MAGVIT2-XL (Luo et al., 2024)	AR	1.5B	2.33	271.8	0.84	0.54
VAR-d16 (Tian et al., 2024)	AR	310M	3.30	274.4	0.84	0.51
VAR-d20 (Tian et al., 2024)	AR	600M	2.57	302.6	0.83	0.56
VAR-d24 (Tian et al., 2024)	AR	1.0B	2.09	312.9	0.82	0.59
MAGE (Li et al., 2023b)	AR	230M	6.93	195.8	-	-
MaskGIT (Chang et al., 2022)	AR	227M	6.18	182.1	0.80	0.51
FlowMo-Lo (Sargent et al., 2025)	AR	397M	4.30	274.0	0.86	0.47
SemTok-AR-L (Ours)	AR	318M	2.77	293.1	0.78	0.60
SemTok-AR-XL (Ours)	AR	746M	2.54	305.6	0.78	0.60
SemTok-AR-XXL (Ours)	AR	1.2B	2.34	310.5	0.77	0.63

results shown in Tab. 2. We further explore different sizes of the AR model (from 318M to 1.2B) and observe strong scalability with consistent performance improvements. **Our AR model achieves performance on generation tasks fully comparable to SOTA methods VAR (Tian et al., 2024), LlamaGen (Sun et al., 2024), and RandAR (Pang et al., 2025).** Notably, compared to MaskGIT (Chang et al., 2022) and MAGE (Li et al., 2023b), which are also based on masked autoregressive modeling with classical 2D tokenizers, our SemTok-based approach significantly advances the generation quality of this paradigm. Those results validate the scalability of 1D semantic representations for downstream tasks, enabling tighter global modeling in the autoregressive process through more compact semantic tokens.

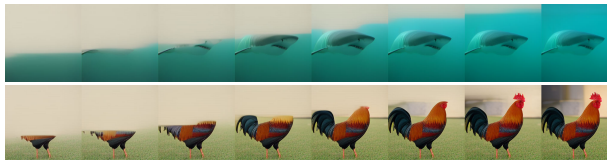
4.4. Ablation Study

Generation with different tokenizers. In Tab. 3, we compare SemTok against two baseline tokenizers on image gen-

Table 3. Generation results of different tokenizers on ImageNet (256 × 256).

Tokenizer	Type	gFID↓	IS ↑	Pre↑	Rec↑
VQGAN (Esser et al., 2021)	2D	4.62	254.1	0.84	0.49
FlowMo-Lo (Sargent et al., 2025)	1D	6.68	280.4	0.82	0.45
SemTok (Ours)	1D	2.77	293.1	0.78	0.60

Progressive generations in raster order *with 2D tokens: VQGAN*



Progressive generations in raster order *with 1D tokens: SemTok*



Figure 5. Progressive generation results in raster scan order between 1D and 2D tokens.

eration using the same AR framework. **SemTok significantly outperforms both 2D grid-based VQGAN (Esser et al., 2021) and previous 1D-based FlowMo-Lo (Sargent et al., 2025).** The superiority of SemTok aligns with our view that 1D representations capture global semantics unbound by spatial structure, enabling richer and more coherent autoregressive generation. Further boosted by *semantic alignment constraint* and *generative training strategy*, SemTok learns more compact, high-level visual representations, yielding better downstream performance.

We visualize generated samples based on VQGAN and SemTok tokenizers in Fig. 6, demonstrating that SemTok produces high-quality images with superior fidelity and diversity. To further highlight the semantic distinction between 1D and 2D tokens, Fig. 5 visualizes multi-step autoregressive generation using raster-order decoding. 2D tokens follow a rigid spatial pattern, with each token encoding

Table 4. Ablation on the *Semantic Alignment Constraint*.

Constraint		Reconstruction		Generation	
Contrastive	Distill	rFID↓	PSNR↑	gFID↓	IS ↑
✗	✗	1.08	21.74	3.83	271.4
✓	✗	0.97	21.86	2.87	276.8
✗	✓	1.02	21.79	3.55	264.9
✓	✓	0.88	22.19	2.77	293.1

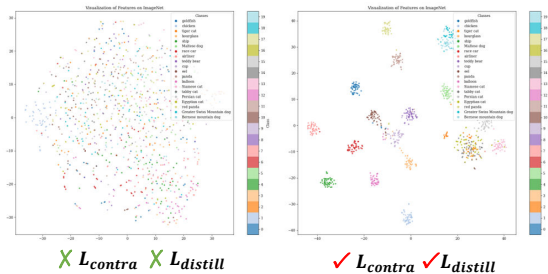


Figure 6. Feature Clustering with different loss functions.

only local content, while 1D tokens progressively refine global semantics without spatial constraints. This aligns with our view that 1D semantic encoding compresses global semantics, yielding more compact and semantic-preserved representations.

Semantic Alignment Constraint. In Tab. 4, we compare the results of applying versus not applying the *semantic alignment constraint* on dual branches of the encoder. The constraints on both branches consistently improve both reconstruction and downstream generation performance. Furthermore, we visualize the clustering of encoder features (*i.e.*, the layer immediately preceding token compression) in the embedding space under different settings. As shown, applying the *semantic alignment constraint* leads to clear clustering of features in the embedding space, indicating that key semantic concepts are explicitly preserved and emphasized. By aligning learned tokens with high-level semantic features from a pretrained vision model, our constraint guides the tokenizer to preserve meaningful visual concepts over low-level artifacts, enhancing semantic fidelity and bridging discrete tokenization with high-level visual understanding.

Non-sequential modeling. Our SemTok adopts a non-sequential modeling approach and employs a masked autoregressive framework for image generation. In Tab. 5, we compare against the sequential 1D tokenization in SelfTok (Wang et al., 2025), which generates tokens autoregressively via next-token prediction. Non-sequential modeling achieves superior results in both image reconstruction and generation, as it respects the inherent global semantic complementarity among tokens, enables more effective modeling of global correlations, and eliminates the inductive bias introduced by arbitrary token ordering. We argue that

Table 5. Ablation on the *Masked Autoregressive Modeling vs. Next-token Prediction*.

Order	Reconstruction		Generation	
	rFID↓	PSNR↑	gFID↓	IS ↑
Raster	1.22	21.07	3.08	269.9
Global	0.88	22.19	2.77	293.1

Table 6. Ablation on the *Two-stage Training Strategy*.

Tokenizer	#Codebook	rFID↓	PSNR ↑	SSIM↑	LPIPS↓
Diffusion	2^{18}	1.31	20.48	0.580	0.177
Refiner	2^{18}	0.88	22.19	0.639	0.128
Diffusion	2^{32}	1.03	21.43	0.633	0.145
Refiner	2^{32}	0.67	23.05	0.684	0.100



Table 7. Reconstructions of diffusion sampler and one-step refiner.

imposing additional sequential constraints compromises the information density of the compressed sequence and hinders its ability to model long-range dependencies.

Two-stage Training Strategy. In Tab. 6, we verify the effectiveness of our two-stage training strategy. After Stage II training, the one-step refiner achieves consistently improved reconstruction over the initial diffusion sampler, particularly in pixel-level fidelity metrics such as PSNR and SSIM, indicating richer texture and finer details. In Fig. 7, we visualize the reconstruction results of the one-step refiner and diffusion sampler. Beyond better preserving semantics and generating finer details, the one-step refiner produces consistently realistic content while avoiding the inconsistency caused by the inherent randomness of diffusion sampling.

5. Conclusion

To achieve compact and semantic-rich visual representations, we proposed SemTok, a novel visual tokenizer that compresses 2D images into 1D sequences. Through 2D-to-1D conversion, semantic alignment constraint, and generative training, SemTok delivered top-tier image reconstruction with compact compression. Leveraging SemTok, we developed a masked AR framework for downstream image generation, with extensive experiments validating its performance in both tokenization and high-level tasks.

Impact Statement

This paper presents work whose goal is to advance the field of Machine Learning. There are many potential societal consequences of our work, none of which we feel must be specifically highlighted here.

References

- Agarwal, N., Ali, A., Bala, M., Balaji, Y., Barker, E., Cai, T., Chattopadhyay, P., Chen, Y., Cui, Y., Ding, Y., et al. Cosmos world foundation model platform for physical ai. *arXiv preprint arXiv:2501.03575*, 2025.
- Bachmann, R., Allardice, J., Mizrahi, D., Fini, E., Kar, O. F., Amirloo, E., El-Nouby, A., Zamir, A., and Dehghan, A. Flextok: Resampling images into 1d token sequences of flexible length. In *Forty-second International Conference on Machine Learning*, 2025.
- Bengio, Y., Léonard, N., and Courville, A. Estimating or propagating gradients through stochastic neurons for conditional computation. *arXiv preprint arXiv:1308.3432*, 2013.
- Brock, A., Donahue, J., and Simonyan, K. Large scale gan training for high fidelity natural image synthesis. *arXiv preprint arXiv:1809.11096*, 2018.
- Chang, H., Zhang, H., Jiang, L., Liu, C., and Freeman, W. T. Maskgit: Masked generative image transformer. In *Proceedings of the IEEE/CVF conference on computer vision and pattern recognition*, pp. 11315–11325, 2022.
- Chang, H., Zhang, H., Barber, J., Maschinot, A., Lezama, J., Jiang, L., Yang, M., Murphy, K. P., Freeman, W. T., Rubinstein, M., Li, Y., and Krishnan, D. Muse: Text-to-image generation via masked generative transformers. In *ICML*, volume 202 of *Proceedings of Machine Learning Research*, pp. 4055–4075. PMLR, 2023.
- Chen, J., Yu, J., Ge, C., Yao, L., Xie, E., Wu, Y., Wang, Z., Kwok, J., Luo, P., Lu, H., et al. Pixart- α : Fast training of diffusion transformer for photorealistic text-to-image synthesis. *arXiv preprint arXiv:2310.00426*, 2023.
- Chen, Y., Girdhar, R., Wang, X., Rambhatla, S. S., and Misra, I. Diffusion autoencoders are scalable image tokenizers. *arXiv preprint arXiv:2501.18593*, 2025.
- Dehghani, M., Djolonga, J., Mustafa, B., Padlewski, P., Heek, J., Gilmer, J., Steiner, A. P., Caron, M., Geirhos, R., Alabdulmohsin, I., et al. Scaling vision transformers to 22 billion parameters. In *International conference on machine learning*, pp. 7480–7512. PMLR, 2023.
- Deng, J., Dong, W., Socher, R., Li, L.-J., Li, K., and Fei-Fei, L. Imagenet: A large-scale hierarchical image database. In *2009 IEEE conference on computer vision and pattern recognition*, pp. 248–255. Ieee, 2009.
- Devlin, J., Chang, M., Lee, K., and Toutanova, K. BERT: pre-training of deep bidirectional transformers for language understanding. In *NAACL-HLT (1)*, pp. 4171–4186. Association for Computational Linguistics, 2019.
- Dhariwal, P. and Nichol, A. Diffusion models beat gans on image synthesis. *Advances in neural information processing systems*, 34:8780–8794, 2021a.
- Dhariwal, P. and Nichol, A. Q. Diffusion models beat gans on image synthesis. In *NeurIPS*, pp. 8780–8794, 2021b.
- Esser, P., Rombach, R., and Ommer, B. Taming transformers for high-resolution image synthesis. In *Proceedings of the IEEE/CVF conference on computer vision and pattern recognition*, pp. 12873–12883, 2021.
- Esser, P., Kulal, S., Blattmann, A., Entezari, R., Müller, J., Saini, H., Levi, Y., Lorenz, D., Sauer, A., Boesel, F., et al. Scaling rectified flow transformers for high-resolution image synthesis. In *Forty-first international conference on machine learning*, 2024.
- Ge, Y., Zhao, S., Zhu, J., Ge, Y., Yi, K., Song, L., Li, C., Ding, X., and Shan, Y. Seed-x: Multimodal models with unified multi-granularity comprehension and generation. *arXiv preprint arXiv:2404.14396*, 2024.
- Goodfellow, I., Pouget-Abadie, J., Mirza, M., Xu, B., Warde-Farley, D., Ozair, S., Courville, A., and Bengio, Y. Generative adversarial networks. *Communications of the ACM*, 63(11):139–144, 2020.
- Han, J., Liu, J., Jiang, Y., Yan, B., Zhang, Y., Yuan, Z., Peng, B., and Liu, X. Infinity: Scaling bitwise autoregressive modeling for high-resolution image synthesis. In *Proceedings of the Computer Vision and Pattern Recognition Conference*, pp. 15733–15744, 2025.
- He, K., Zhang, X., Ren, S., and Sun, J. Deep residual learning for image recognition. In *Proceedings of the IEEE conference on computer vision and pattern recognition*, pp. 770–778, 2016.
- He, K., Chen, X., Xie, S., Li, Y., Dollár, P., and Girshick, R. Masked autoencoders are scalable vision learners. In *Proceedings of the IEEE/CVF conference on computer vision and pattern recognition*, pp. 16000–16009, 2022.
- Heusel, M., Ramsauer, H., Unterthiner, T., Nessler, B., and Hochreiter, S. Gans trained by a two time-scale update rule converge to a local nash equilibrium. *Advances in neural information processing systems*, 30, 2017.
- Ho, J. and Salimans, T. Classifier-free diffusion guidance. *arXiv preprint arXiv:2207.12598*, 2022.

- Ho, J., Jain, A., and Abbeel, P. Denoising diffusion probabilistic models. *Advances in neural information processing systems*, 33:6840–6851, 2020.
- Hoogeboom, E., Heek, J., and Salimans, T. simple diffusion: End-to-end diffusion for high resolution images. In *ICML*, volume 202 of *Proceedings of Machine Learning Research*, pp. 13213–13232. PMLR, 2023.
- Jansen, A., Ellis, D. P., Hershey, S., Moore, R. C., Plakal, M., Popat, A. C., and Saurous, R. A. Coincidence, categorization, and consolidation: Learning to recognize sounds with minimal supervision. In *ICASSP 2020-2020 IEEE International Conference on Acoustics, Speech and Signal Processing (ICASSP)*, pp. 121–125. IEEE, 2020.
- Jin, Y., Xu, K., Xu, K., Chen, L., Liao, C., Tan, J., Huang, Q., Chen, B., Song, C., Meng, D., Zhang, D., Ou, W., Gai, K., and Mu, Y. Unified language-vision pretraining in LLM with dynamic discrete visual tokenization. In *ICLR*. OpenReview.net, 2024.
- Kang, M., Zhu, J.-Y., Zhang, R., Park, J., Shechtman, E., Paris, S., and Park, T. Scaling up gans for text-to-image synthesis. In *Proceedings of the IEEE/CVF conference on computer vision and pattern recognition*, pp. 10124–10134, 2023.
- Karras, T., Laine, S., and Aila, T. A style-based generator architecture for generative adversarial networks. In *Proceedings of the IEEE/CVF conference on computer vision and pattern recognition*, pp. 4401–4410, 2019.
- Kingma, D. P. and Gao, R. Understanding diffusion objectives as the ELBO with simple data augmentation. In *NeurIPS*, 2023.
- Kingma, D. P. and Welling, M. Auto-encoding variational bayes. *arXiv preprint arXiv:1312.6114*, 2013.
- Kynkäänniemi, T., Karras, T., Laine, S., Lehtinen, J., and Aila, T. Improved precision and recall metric for assessing generative models. *Advances in neural information processing systems*, 32, 2019.
- Lee, D., Kim, C., Kim, S., Cho, M., and Han, W.-S. Autoregressive image generation using residual quantization. In *Proceedings of the IEEE/CVF conference on computer vision and pattern recognition*, pp. 11523–11532, 2022.
- Li, J., Li, D., Savarese, S., and Hoi, S. Blip-2: Bootstrapping language-image pre-training with frozen image encoders and large language models. In *International conference on machine learning*, pp. 19730–19742. PMLR, 2023a.
- Li, T., Chang, H., Mishra, S., Zhang, H., Katabi, D., and Krishnan, D. Mage: Masked generative encoder to unify representation learning and image synthesis. In *Proceedings of the IEEE/CVF Conference on Computer Vision and Pattern Recognition*, pp. 2142–2152, 2023b.
- Li, T., Tian, Y., Li, H., Deng, M., and He, K. Autoregressive image generation without vector quantization. *Advances in Neural Information Processing Systems*, 37:56424–56445, 2024.
- Lipman, Y., Chen, R. T., Ben-Hamu, H., Nickel, M., and Le, M. Flow matching for generative modeling. *arXiv preprint arXiv:2210.02747*, 2022.
- Liu, H., Li, C., Wu, Q., and Lee, Y. J. Visual instruction tuning. *Advances in neural information processing systems*, 36:34892–34916, 2023a.
- Liu, X., Gong, C., and Liu, Q. Flow straight and fast: Learning to generate and transfer data with rectified flow. In *ICLR*. OpenReview.net, 2023b.
- Luo, Z., Shi, F., Ge, Y., Yang, Y., Wang, L., and Shan, Y. Open-magvit2: An open-source project toward democratizing auto-regressive visual generation. *arXiv preprint arXiv:2409.04410*, 2024.
- Ma, C., Jiang, Y., Wu, J., Yang, J., Yu, X., Yuan, Z., Peng, B., and Qi, X. Unitok: A unified tokenizer for visual generation and understanding. *arXiv preprint arXiv:2502.20321*, 2025.
- Mentzer, F., Minnen, D., Agustsson, E., and Tschannen, M. Finite scalar quantization: Vq-vae made simple. *arXiv preprint arXiv:2309.15505*, 2023.
- Pang, Z., Zhang, T., Luan, F., Man, Y., Tan, H., Zhang, K., Freeman, W. T., and Wang, Y.-X. Randar: Decoder-only autoregressive visual generation in random orders. In *Proceedings of the Computer Vision and Pattern Recognition Conference*, pp. 45–55, 2025.
- Peebles, W. and Xie, S. Scalable diffusion models with transformers. In *ICCV*, pp. 4172–4182. IEEE, 2023.
- Radford, A., Kim, J. W., Hallacy, C., Ramesh, A., Goh, G., Agarwal, S., Sastry, G., Askell, A., Mishkin, P., Clark, J., et al. Learning transferable visual models from natural language supervision. In *International conference on machine learning*, pp. 8748–8763. Pmlr, 2021.
- Ramesh, A., Pavlov, M., Goh, G., Gray, S., Voss, C., Radford, A., Chen, M., and Sutskever, I. Zero-shot text-to-image generation. In *International conference on machine learning*, pp. 8821–8831. Pmlr, 2021.
- Razavi, A., Van den Oord, A., and Vinyals, O. Generating diverse high-fidelity images with vq-vae-2. *Advances in neural information processing systems*, 32, 2019.

- Rombach, R., Blattmann, A., Lorenz, D., Esser, P., and Ommer, B. High-resolution image synthesis with latent diffusion models. In *Proceedings of the IEEE/CVF conference on computer vision and pattern recognition*, pp. 10684–10695, 2022.
- Salimans, T., Goodfellow, I., Zaremba, W., Cheung, V., Radford, A., and Chen, X. Improved techniques for training gans. *Advances in neural information processing systems*, 29, 2016.
- Sargent, K., Hsu, K., Johnson, J., Fei-Fei, L., and Wu, J. Flow to the mode: Mode-seeking diffusion autoencoders for state-of-the-art image tokenization. *arXiv preprint arXiv:2503.11056*, 2025.
- Su, J., Ahmed, M., Lu, Y., Pan, S., Bo, W., and Liu, Y. Roformer: Enhanced transformer with rotary position embedding. *Neurocomputing*, 568:127063, 2024.
- Sun, P., Jiang, Y., Chen, S., Zhang, S., Peng, B., Luo, P., and Yuan, Z. Autoregressive model beats diffusion: Llama for scalable image generation. *arXiv preprint arXiv:2406.06525*, 2024.
- Sun, Q., Yu, Q., Cui, Y., Zhang, F., Zhang, X., Wang, Y., Gao, H., Liu, J., Huang, T., and Wang, X. Emu: Generative pretraining in multimodality. *arXiv preprint arXiv:2307.05222*, 2023.
- Tian, K., Jiang, Y., Yuan, Z., Peng, B., and Wang, L. Visual autoregressive modeling: Scalable image generation via next-scale prediction. *Advances in neural information processing systems*, 37:84839–84865, 2024.
- Tschannen, M., Gritsenko, A., Wang, X., Naeem, M. F., Alabdulmohsin, I., Parthasarathy, N., Evans, T., Beyer, L., Xia, Y., Mustafa, B., et al. Siglip 2: Multilingual vision-language encoders with improved semantic understanding, localization, and dense features. *arXiv preprint arXiv:2502.14786*, 2025.
- Van Den Oord, A., Vinyals, O., et al. Neural discrete representation learning. *Advances in neural information processing systems*, 30, 2017.
- Wang, B., Yue, Z., Zhang, F., Chen, S., Bi, L., Zhang, J., Song, X., Chan, K. Y., Pan, J., Wu, W., et al. Selftok: Discrete visual tokens of autoregression, by diffusion, and for reasoning. *arXiv preprint arXiv:2505.07538*, 2025.
- Wang, X., Zhang, X., Luo, Z., Sun, Q., Cui, Y., Wang, J., Zhang, F., Wang, Y., Li, Z., Yu, Q., et al. Emu3: Next-token prediction is all you need. *arXiv preprint arXiv:2409.18869*, 2024.
- Weber, M., Yu, L., Yu, Q., Deng, X., Shen, X., Cremers, D., and Chen, L. Maskbit: Embedding-free image generation via bit tokens. *Trans. Mach. Learn. Res.*, 2024, 2024.
- Xie, J., Mao, W., Bai, Z., Zhang, D. J., Wang, W., Lin, K. Q., Gu, Y., Chen, Z., Yang, Z., and Shou, M. Z. Show-o: One single transformer to unify multimodal understanding and generation. *arXiv preprint arXiv:2408.12528*, 2024.
- Yang, Z., Teng, J., Zheng, W., Ding, M., Huang, S., Xu, J., Yang, Y., Hong, W., Zhang, X., Feng, G., Yin, D., Zhang, Y., Wang, W., Cheng, Y., Xu, B., Gu, X., Dong, Y., and Tang, J. Cogvideox: Text-to-video diffusion models with an expert transformer. In *ICLR*. OpenReview.net, 2025.
- Yao, J., Yang, B., and Wang, X. Reconstruction vs. generation: Taming optimization dilemma in latent diffusion models. In *Proceedings of the Computer Vision and Pattern Recognition Conference*, pp. 15703–15712, 2025.
- Yu, J., Li, X., Koh, J. Y., Zhang, H., Pang, R., Qin, J., Ku, A., Xu, Y., Baldrige, J., and Wu, Y. Vector-quantized image modeling with improved vqgan. *arXiv preprint arXiv:2110.04627*, 2021.
- Yu, J., Li, X., Koh, J. Y., Zhang, H., Pang, R., Qin, J., Ku, A., Xu, Y., Baldrige, J., and Wu, Y. Vector-quantized image modeling with improved VQGAN. In *ICLR*. OpenReview.net, 2022a.
- Yu, J., Xu, Y., Koh, J. Y., Luong, T., Baid, G., Wang, Z., Vasudevan, V., Ku, A., Yang, Y., Ayan, B. K., et al. Scaling autoregressive models for content-rich text-to-image generation. *arXiv preprint arXiv:2206.10789*, 2(3):5, 2022b.
- Yu, L., Lezama, J., Gundavarapu, N. B., Versari, L., Sohn, K., Minnen, D., Cheng, Y., Birodkar, V., Gupta, A., Gu, X., et al. Language model beats diffusion—tokenizer is key to visual generation. *arXiv preprint arXiv:2310.05737*, 2023.
- Yu, Q., Weber, M., Deng, X., Shen, X., Cremers, D., and Chen, L.-C. An image is worth 32 tokens for reconstruction and generation. *Advances in Neural Information Processing Systems*, 37:128940–128966, 2024.
- Yu, Q., He, J., Deng, X., Shen, X., and Chen, L.-C. Randomized autoregressive visual generation. In *Proceedings of the IEEE/CVF International Conference on Computer Vision (ICCV)*, pp. 18431–18441, October 2025.
- Zhai, X., Mustafa, B., Kolesnikov, A., and Beyer, L. Sigmoid loss for language image pre-training. In *Proceedings of the IEEE/CVF international conference on computer vision*, pp. 11975–11986, 2023.
- Zhang, R., Isola, P., Efros, A. A., Shechtman, E., and Wang, O. The unreasonable effectiveness of deep features as a perceptual metric. In *Proceedings of the IEEE conference on computer vision and pattern recognition*, pp. 586–595, 2018.

Zhao, Y., Xiong, Y., and Krähenbühl, P. Image and video tokenization with binary spherical quantization. *arXiv preprint arXiv:2406.07548*, 2024.

Zhao, Y., Xue, F., Reed, S., Fan, L., Zhu, Y., Kautz, J., Yu, Z., Krähenbühl, P., and Huang, D.-A. Qlip: Text-aligned visual tokenization unifies auto-regressive multimodal understanding and generation. *arXiv preprint arXiv:2502.05178*, 2025.

Zheng, B., Ma, N., Tong, S., and Xie, S. Diffusion transformers with representation autoencoders. *arXiv preprint arXiv:2510.11690*, 2025.

Zheng, C., Vuong, T.-L., Cai, J., and Phung, D. Movq: Modulating quantized vectors for high-fidelity image generation. *Advances in Neural Information Processing Systems*, 35:23412–23425, 2022.

A. Implementation Details

A.1. Details of the SemTok Tokenizer

Table 8. Architecture Configuration of SemTok.

Model	Depth	Width	Heads	# Params
Encoder	8	768	12	113M
Decoder	24	1536	24	2236M

Encoder. Our encoder follows an MMDiT-based (Esser et al., 2024) architecture. Drawing on the findings in FlowMo (Sargent et al., 2025), we argue that a lightweight encoder is sufficient to accomplish the compression and representation of image semantics, where the configuration is listed in 8. Images are first compressed into latents using SD3.5-VAE (Rombach et al., 2022) with a downscale factor of 8. Both the encoder and decoder operate on 2×2 patches of VAE latents to reduce the sequence lengths. We apply 2D RoPE (Su et al., 2024) and 1D RoPE to represent positional relationships of 2D image tokens and 1D semantic tokens, respectively.

Decoder. We argue that, as a generator, the decoder is tasked with reconstructing raw pixels from the compressed sequence, and thus requires a large architecture to learn the generation prior. We thus adopt SD3.5 (Esser et al., 2024) for the decoder and initialize it with its pre-trained parameters to inherit robust generation capabilities, where the configuration is listed in 8. Consistent with the encoder, we apply 2D and 1D RoPE to the two branches of the decoder as well. The predicted latents are mapped back to raw pixels via the VAE decoder.

Other Configuration. For data augmentation, we resize the input image to 256×256 and apply horizontal flipping. In Stage I, we utilize the uniform noise distribution schedule on $[0, 1]$ for rectified flow training. During inference, SemTok predicts images from noise through 25-step iteration with a sampler in (Esser et al., 2024). In Stage II, we adopt the same discriminator as that in (Weber et al., 2024), which is incorporated after 20,000 iterations with the learning rate set to 1×10^{-4} . The learning rate is warmed up over the first 10,000 iterations and scheduled following cosine annealing. We use the exponential moving average (EMA) with a rate of 0.9999. In all ablation experiments, we employ SemTok with a codebook size of 2^{18} to accelerate the convergence rate under limited computational resources.

A.2. Details of the Autoregressive Framework

Table 9. Architecture Configuration of the AR model.

Size	Depth	Width	Heads	# Params
L	24	1024	16	318M
XL	36	1280	20	746M
XXL	24	2048	32	1.2B

Model Architecture. We employ SemTok with a codebook size of 2^{18} as the basic visual tokenizer. Our AR model follows the architecture of LlamaGen (Sun et al., 2024) with 1D RoPE (Su et al., 2024). Our model employs a bidirectional attention mechanism for global correlations, unlike the original model with a causal mask. We employ QK normalization (Dehghani et al., 2023) to stabilize training. In Tab. 9, we scale the model size from 318M up to 1.2B parameters following previous works (Sun et al., 2024). For class-conditioned image generation, we concatenate the learnable class token with the image tokens and place it at the beginning. Additionally, it serves as a condition through AdaLN (Peebles & Xie, 2023). Given the large codebook size of our tokenizer to enhance its representational capacity, a conventional classifier would demand substantial storage space. We therefore adopt the Infinite-Vocabulary Classifier (IVC) in (Han et al., 2025), which performs binary classification on each index bit to accelerate convergence.

Inference. Our AR model predicts several tokens from masked tokens progressively in a fully randomized order, with the masking ratio following a cosine schedule. This enables us to predict multiple tokens in parallel at each step, with 64 steps set as the default to generate 256 tokens. We adopt top- p based filtering techniques, since our bitwise classifier only supports binary sampling for each bit. We sweep the optimal top- p value and set it to 0.75.

Other Configuration. We apply a dropout probability of 0.1 on the class condition to adopt CFG (Ho & Salimans, 2022). We use a simple linear CFG schedule, where the scale rises linearly to its maximum based on the ratio of predicted tokens. We sweep the optimal guidance scale for each model with 6.0 for SemTok-AR-L, 5.3 for SemTok-AR-XL, and 4.9 for SemTok-AR-XXL. We adopt label smoothing with a factor of 0.01 to enhance the generalization. In all ablation experiments, we employ AR model-L to accelerate the convergence rate under limited computational resources.

B. Additional Experimental Results

B.1. Ablation Study of SemTok Tokenizer

Table 10. Ablation on the *Quantizer*.

Quantizer	rFID↓	PSNR ↑	SSIM↑	LPIPS↓
LFQ (Yu et al., 2023)	1.32	20.78	0.564	0.163
BSQ (Zhao et al., 2024)	0.88	22.19	0.639	0.128

Binary Spherical Quantizer. Our SemTok adopts BSQ (Zhao et al., 2024) as the quantizer, which projects the high-dimensional visual embedding to a lower-dimensional hypersphere and applies binary quantization without requiring extra space for codebook storage in VQ (Van Den Oord et al., 2017). Compared with LFQ (Yu et al., 2023), BSQ enables efficient entropy calculation via soft quantization and bounds quantization errors through \mathcal{L}_2 normalization, thus achieving faster and better convergence. As shown in Tab. 10, BSQ achieves superior results in image reconstruction tasks, verifying its stronger generalization and adaptability.

Table 11. Ablation on the *Perceptual Loss*.

\mathcal{L}_{per}	rFID↓	PSNR ↑	SSIM↑	LPIPS↓
LPIPS (Zhang et al., 2018)	1.13	22.73	0.649	0.133
ResNet (He et al., 2016)	0.89	22.02	0.622	0.133
LPIPS + ResNet	0.88	22.19	0.639	0.128

Perceptual Loss. Previous works (Weber et al., 2024; Sargent et al., 2025) verify the effectiveness of ResNet-based (He et al., 2016) perceptual loss for image tokenization. Compared with LPIPS (Zhang et al., 2018), which uses intermediate feature distance loss to enhance the similarity between local features, the ResNet loss based on logits is more capable of focusing on the fidelity of high-level semantics in reconstruction. We consider both perspectives important for visual tokenization. Thus, unlike (Weber et al., 2024; Sargent et al., 2025), we sum these two losses as the overall perceptual loss. In Tab. 11, the joint application of both losses yields superior results compared with using a single loss. Furthermore, LPIPS loss focuses on improving local fidelity metrics such as SSIM, while ResNet loss targets metrics like rFID that reflect semantic distribution similarity, which aligns with our expectations.

Table 12. Ablation on the *Generative Training Strategy*.

Stage	rFID↓	PSNR ↑	SSIM↑	LPIPS↓
Only Fine-tuning	1.80	20.54	0.556	0.177
Pre-training & Fine-tuning	0.88	22.19	0.639	0.128

Generative Training Strategy. Our SemTok utilizes a two-stage generative training strategy to explore a richer semantic distribution in the latent space. Specifically, Stage I drives generative space exploration via a diffusion-based decoder, which searches for optimal sampling paths from randomly distributed noise to achieve superior semantic representation. In contrast, Stage II fine-tuning aligns with the classical pixel-level reconstruction pipeline, focusing on detail refinement rather than further modeling of semantic distribution. In Tab. 12, models incorporating generative pre-training yield significantly superior performance compared to only fine-tuning. Tab. 6 and Tab. 12 show that Stage I enhances semantic understanding, while Stage II ensures local detail fidelity. Their synergy resolves the semantic-detail trade-off, ultimately leading to enhanced performance in visual tokenization tasks.

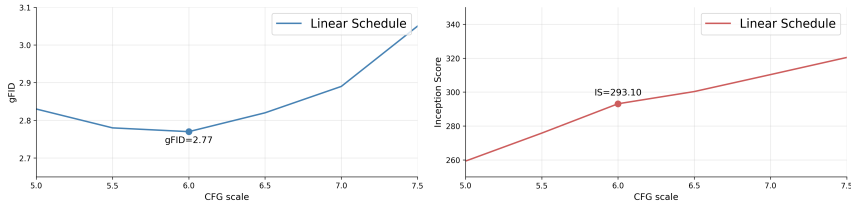


Figure 7. The influence of CFG scale under *Linear Schedule*.

B.2. Ablation Study of Autoregressive Framework

CFG Scale. Our AR model incorporates CFG (Ho & Salimans, 2022) to boost generation quality, which imposes guidance on the sampling procedure, thereby shifting the distribution toward more desirable characteristics. We dynamically adjust the CFG scale via a linear schedule during iterative sampling, and identify its optimal value through systematic search over predefined candidates, which is shown in Fig. 7. Increasing the CFG scale continuously improves generation quality (*i.e.*, Inception Score), whereas its impact on gFID shows a non-monotonic trend of initial decline then enhancement.

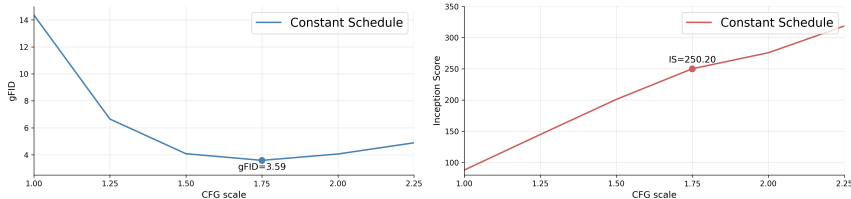


Figure 8. The influence of CFG scale under *Constant Schedule*.

CFG Schedule. We compare the linear schedule of CFG against the classic constant schedule, with the search results for the latter presented in Fig. 8 (scale=1.0 denotes without CFG). The variation trend of the constant schedule is similar to that of the linear schedule, but its optimal performance is inferior. We argue that a gradual increase schedule in CFG scale during iterations is more optimal, since the autoregressive process suffers from insufficient prior information in its early stage, where an excessively large CFG scale may cause distributional over-shifting or collapse.

Table 13. Ablation on the *Bitwise Classifier*.

Groups of Codebook	gFID↓	IS ↑	Pre↑	Rec↑
2	4.77	251.4	0.76	0.48
18 (Bitwise)	2.77	293.1	0.78	0.60

Bitwise Classifier. We use a bitwise classifier to predict bit labels, equivalent to partitioning the codebook with size $|\mathcal{C}|$ into $\log_2 |\mathcal{C}|$ groups. We compare this approach with the classifier that partitions the codebook into only 2 groups and predicts index labels under a codebook size of 2^{18} , since a large vocabulary size would lead to excessive memory overhead for conventional classifiers. As shown in Tab. 13, the bit-wise classifier achieves superior generation performance and faster convergence. We argue that this effectiveness to the BSQ of the codebook. As analyzed in (Weber et al., 2024), BSQ imparts structured semantics to bit-token representations: adjacent tokens (Hamming distance = 1) are semantically similar, and flipping bits does not induce substantial semantic changes.

Sampling Strategy. Our AR model follows the same design as MAR (Li et al., 2024), employing a fully randomized order to predict tokens at different positions. This randomized order differs from that of masked autoregressive methods such as MaskGIT (Chang et al., 2022) and MAGE (Li et al., 2023b), where the positions of the next tokens to predict are dynamically determined by their confidence. In other words, this confidence-based sampling strategy prioritizes predicting tokens with higher confidence. As shown in Tab. 14, the random sampling strategy achieves better gFID performance, as its random order induces more diverse prediction distributions.

Table 14. Ablation on the Sampling Strategy.

Strategy	gFID↓	IS↑	Pre↑	Rec↑
Confidence-based	3.60	246.8	0.74	0.62
Random	2.77	293.1	0.78	0.60

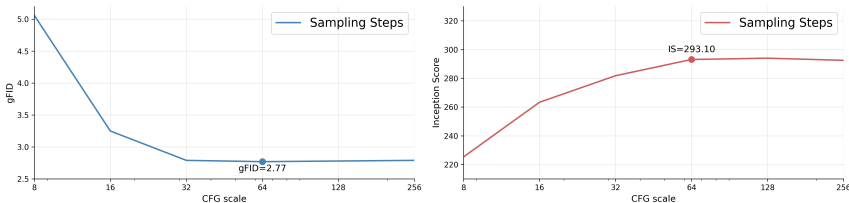


Figure 9. Ablation on the Sampling Steps for token generation.

Sampling Steps. AR models based on next-token prediction can only generate one token per inference step, making the number of steps a critical factor affecting computational efficiency. Our masked autoregressive modeling enables bidirectional token dependencies, allowing multiple tokens to be generated in parallel. Thus, we can improve generation speed by reducing sampling steps. As shown in Fig. 9, once the sampling steps reach 64, additional steps yield only marginal improvements. We argue that 64 steps represent an optimal trade-off between speed and accuracy.

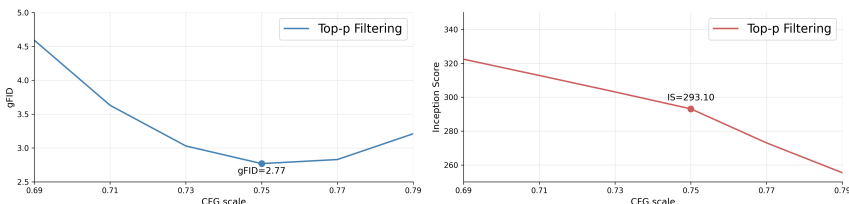


Figure 10. Ablation on the Top-p Filtering for token generation.

Top-p Filtering. Based on our bitwise classifier, we apply a top- p based filtering strategy to each bit of the vector index, retaining only those bit categories whose cumulative probability exceeds p . A larger p ensures generation diversity, while a smaller p guarantees image quality. As shown in Fig. 10, we find that $p = 0.75$ strikes the best balance with the lowest gFid. We use the same hyperparameter settings across all experiments.

B.3. Limitations

In this work, we propose SemTok, a novel semantic one-dimensional tokenizer that compresses 2D into 1D discrete tokens with high-level semantics. Despite its strong performance in image reconstruction, its main limitation is that mapping tokens back to raw pixels requires a large generative model (*i.e.*, total 2.3B), which limits inference speed. Although we significantly reduce inference time by pre-compressing images with VQ-VAE and simplifying inference steps via a one-step refiner, further efficiency gains for integrating with VLMs will require exploring lightweight models or techniques.

Moreover, due to limitations in computational resources and time, we only evaluate SemTok on image reconstruction and class-conditioned image generation tasks. Further validation is needed to assess its scalability and robustness across more diverse tasks, such as visual understanding, text-conditioned image generation, and video modeling. For fair comparison, SemTok is trained only on ImageNet, inheriting its dataset bias, which limits qualitative comparison with approaches trained on larger-scale or commercial datasets.

C. More Visualization Results

In Fig. 11, we provide extended comparisons with other tokenizers on the image reconstruction task, showcasing the robust capability of SemTok in reconstructing high-fidelity images. In Fig. 12, we provide additional visualization results of our SemTok-based AR model on the image generation task, showcasing the robust capability of SemTok in generating high-realistic images.

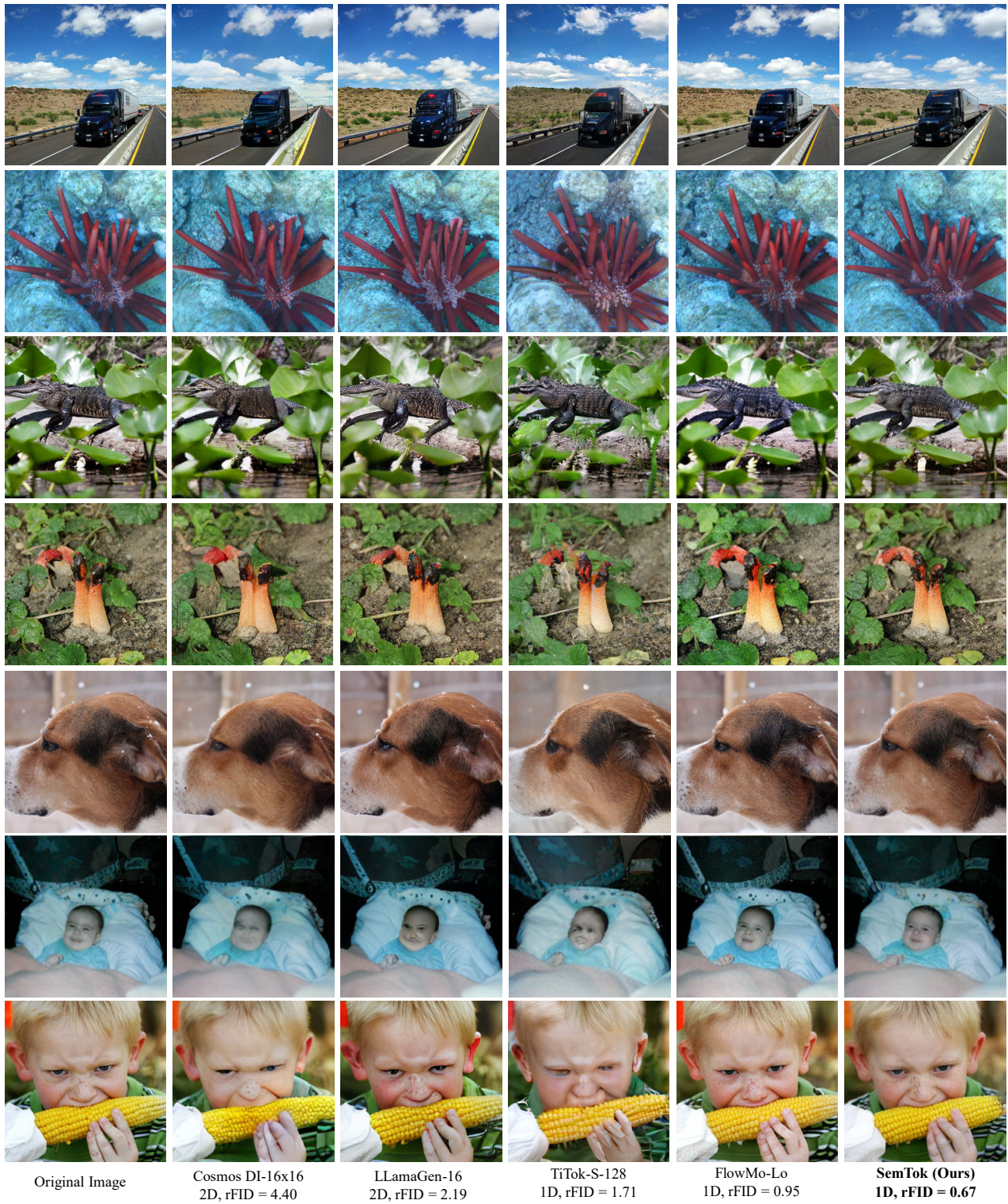


Figure 11. Comparison of reconstructions from different tokenizers.

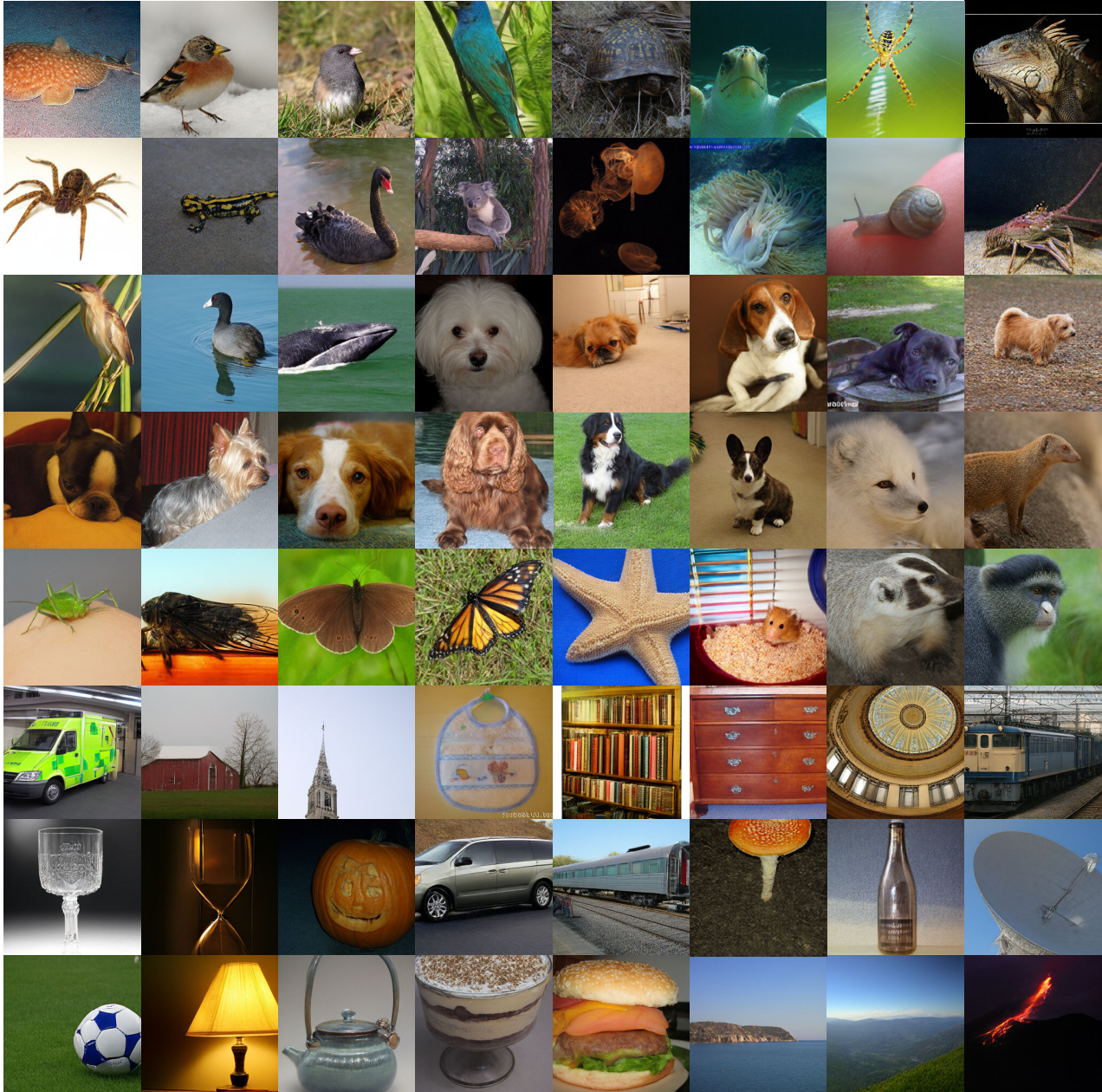


Figure 12. Visualization of generated images from our SemTok-based AR model across random ImageNet classes.